PHOTONICS Research

Circular Bragg lasers with radial PT symmetry: Design and analysis with a coupled-mode approach

Ziyao Feng, Jingwen Ma, Zejie Yu, and Xiankai Sun*

Department of Electronic Engineering, The Chinese University of Hong Kong, Shatin, New Territories, Hong Kong, China
**Corresponding author: xksun@cuhk.edu.hk*

Received 3 November 2017; revised 1 March 2018; accepted 14 March 2018; posted 14 March 2018 (Doc. ID 312603); published 11 April 2018

Parity–time (PT) symmetry has been demonstrated in the frame of classic optics. Its applications in laser science have resulted in unconventional control and manipulation of resonant modes. PT-symmetric periodic circular Bragg lasers were previously proposed. Analyses with a transfer-matrix method have shown their superior properties of reduced threshold and enhanced modal discrimination between the radial modes. However, the properties of the azimuthal modes were not analyzed, which restricts further development of circular Bragg lasers. Here, we adopt the coupled-mode theory to design and analyze chirped circular Bragg lasers with radial PT symmetry. The new structures possess more versatile modal control with further enhanced modal discrimination between the azimuthal modes. We also analyze azimuthally modulated circular Bragg lasers with radial PT symmetry, which are shown to achieve even higher modal discrimination. © 2018 Chinese Laser Press

OCIS codes: (140.4780) Optical resonators; (130.2790) Guided waves; (230.1480) Bragg reflectors; (130.3120) Integrated optics devices.

https://doi.org/10.1364/PRJ.6.000A38

1. INTRODUCTION

Photonic ring and disk resonators have received significant attention because they are widely used for both fundamental research as well as practical applications in optical communications and signal processing [1]. A method to realize high optical quality factors is by confining light to a "defect" region defined by distributed Bragg reflectors. Such resonators are adopted for semiconductor lasers and have been studied with various techniques such as conformal mapping, coupled-wave approach, and transfer-matrix method [2–10]. Previously, much research attention was given to the radial modes, and the effort was focused on designing the structures for larger modal discrimination between modes of different radial orders. In order to achieve single-mode operation, it is equally important to achieve large discrimination between different azimuthal modes. The existing approaches to overcome the challenge include adoption of radially chirped Bragg gratings [7] and azimuthal modulation [8].

"Parity–time (PT) symmetry" was first introduced by Bender *et al.* in quantum mechanics [11]. Due to the similarity between the Schrödinger equation and the Helmholtz equation, the concept of PT symmetry has been adopted in optics [12–14]. The PT-symmetric and PT-broken phases are separated by the exceptional point, where the system's eigenvalues coalesce. Interesting phenomena by mode management around the exceptional points include single-mode lasers [15–20], reversing pump dependence [21–23], orbital angular momentum lasers [24], and unidirectional reflection [25,26].

In 2016, we proposed PT-symmetric circular Bragg lasers with radially periodic gratings. We employed a transfer-matrix method to calculate their reflection and transmission coefficients and analyzed their modal properties [16]. We found enhanced modal discrimination among the radial modes. However, the eigenwaves in circular Bragg lasers take the form of Hankel functions, whose zeros are not equidistantly distributed. In order to achieve perfect phase matching in the radial direction, the phase of the circular gratings of the laser structure has to follow that of the Hankel functions, rendering nonperiodicity (or chirping) in the radial direction. Here, we develop a coupled-mode approach for designing a PT-symmetric circular Bragg laser with the radially chirped gratings. We also investigate the effect of an additional azimuthal modulation of the refractive index and analyze the threshold conditions for different azimuthal modes. The rest of this paper is structured as follows. In Section 2, we focus on radially chirped circular Bragg lasers and derive a set of coupled equations. We compare the threshold gain of conventional and PT-symmetric radially chirped circular Bragg lasers. The PT-symmetric circular Bragg lasers possess the higher modal discrimination. Such lasers are also shown to be highly robust, as a small deviation away from

the exceptional point does not affect the modal discrimination. In Section 3, we include an additional azimuthal modulation to the radially chirped PT-symmetric circular Bragg lasers. By simulating the structures with an finite-difference time-domain (FDTD) method, we find that the structures with an additional azimuthal modulation can effectively suppress other unwanted modes.

2. PT-SYMMETRIC CIRCULAR BRAGG LASERS WITH RADIALLY CHIRPED GRATINGS

We previously proposed a laser structure with its complex refractive index in the radial direction distributed periodically. We used a transfer-matrix method to analyze its threshold gain [16] and found that the threshold gain for different radial modes could have large difference. However, because circular Bragg lasers with radially periodic gratings cannot obtain large modal discrimination between the azimuthal modes [2], here we propose to apply the concept of PT symmetry to radially chirped gratings, as shown in Fig. 1(a). We suggest a structure that possesses the same dispersion relation as that of a planar PT-symmetric grating, where the refractive index distribution along the radial direction is shown in Fig. 1(c). We will compare modal properties of different types of circular Bragg lasers and show that the proposed structure performs better in controlling the azimuthal modes with a high modal discrimination.

Let us consider a specific azimuthal mode with perturbation in the radial direction. Erdogan *et al.* derived the expression for different azimuthal modes of the TE polarization [2]. In contrast with Ref. [2], here we focus our analysis on the TM modes whose major field component is E_z. All the other electromagnetic field components of the TM modes can be obtained from E_z, which satisfies the Helmholtz equation

$$\left[r^2\frac{\partial^2}{\partial r^2}+r\frac{\partial}{\partial r}+\frac{\partial^2}{\partial\varphi^2}+r^2\varepsilon(r,\varphi)k_0^2\right]E_z=0. \tag{1}$$

E_z can generally be expressed as $E_z=\sum_{l=-\infty}^{\infty}E_{zl}\exp(il\varphi)$, where $E_{zl}=A_l(r)H_l^{(1)}(kr)+B_l(r)H_l^{(2)}(kr)$ is the radial distribution of the electric field of the lth-order mode, l is the azimuthal mode number, r and φ are the radial and azimuthal coordinates, respectively, and k is the wavenumber, which becomes k_0 in the vacuum and k_{av} in the medium. The Hankel functions of the first (second) kind represent the radially outward (inward) waves, with A_l and B_l being their amplitudes. With orthogonality of the function $\exp(il\varphi)$, the equation for Hankel-phased circular Bragg resonators was derived by Scheuer *et al.* [8]:

$$\frac{\mathrm{d}A_l}{\mathrm{d}r}(2iH_l^{(1)})-\frac{\mathrm{d}B_l}{\mathrm{d}r}(2iH_l^{(2)})+\frac{k_0\Delta\varepsilon}{n_{\mathrm{av}}}(A_lH_l^{(1)}+B_lH_l^{(2)})=0, \tag{2}$$

where $\Delta\varepsilon(r)$ can be expanded in terms of Hankel functions. The 0th-order Fourier expansion coefficient of $\Delta\varepsilon(r)$ determines how A_l or B_l evolves due to self-contribution, and the ±1st-order coefficients, which contain $\exp[\pm2i\,\mathrm{phase}(H_l^{(1)}(k_{\mathrm{av}}r))]$ terms, determine the strength of coupling between A_l and B_l. In Eq. (2), the derivatives of A_l and B_l can be separated according to their spatial frequency in the radial direction. We suggest the ±1st-order perturbation of $\Delta\varepsilon(r)$ to be $\Delta\varepsilon_r(r)+i\Delta\varepsilon_i(r)$ with

$$\begin{cases}\Delta\varepsilon_r(r)=\Delta\varepsilon_r\cos[2\,\mathrm{phase}(H_l^{(1)}(k_{\mathrm{de}}r))+\theta_1]\\ \Delta\varepsilon_i(r)=\Delta\varepsilon_i\cos[2\,\mathrm{phase}(H_l^{(1)}(k_{\mathrm{de}}r))+\theta_2]\end{cases}, \tag{3}$$

where k_{de} is the spatial frequency of the refractive index modulation. The phase shifts θ_1 and θ_2 are used for satisfying the PT symmetry requirements and for fine-tuning the laser wavelength such that $k_{\mathrm{av}}=k_{\mathrm{de}}$. We define δ as $k_{\mathrm{av}}-k_{\mathrm{de}}$, which is the difference between the actual wavenumber and the designed spatial frequency. With the approximation $H_l^{(1)}(x+\delta x)\approx H_l^{(1)}(x)\exp(i\delta x)$ and separation of the inward and outward waves, the coupled equations for the amplitudes are as follows:

$$\begin{cases}\frac{\mathrm{d}A_l}{\mathrm{d}r}=i\frac{\Delta\varepsilon_r\exp(i\theta_1)+i\Delta\varepsilon_i\exp(i\theta_2)}{4n_{\mathrm{av}}}k_0B_l(r)\exp(-2i\delta r)\\ \frac{\mathrm{d}B_l}{\mathrm{d}r}=-i\frac{\Delta\varepsilon_r\exp(-i\theta_1)+i\Delta\varepsilon_i\exp(-i\theta_2)}{4n_{\mathrm{av}}}k_0A_l(r)\exp(2i\delta r)\end{cases}. \tag{4}$$

The above equations are typical coupled equations for chirped circular Bragg gratings. With $\kappa=\Delta\varepsilon_rk_0/(4n_{\mathrm{av}})$ and $g=\Delta\varepsilon_ik_0/(4n_{\mathrm{av}})$ and expressing $A_l(r)=R_l(r)\exp(-i\delta r)$ and $B_l(r)=S_l(r)\exp(i\delta r)$, we obtain

$$\begin{cases}\frac{\mathrm{d}R_l}{\mathrm{d}r}=i\delta R_l(r)+i(\kappa\exp(i\theta_1)+ig\exp(i\theta_2))S_l(r)\\ \frac{\mathrm{d}S_l}{\mathrm{d}r}=-i(\kappa\exp(-i\theta_1)+ig\exp(-i\theta_2))R_l(r)-i\delta S_l(r)\end{cases}. \tag{5}$$

By expressing $R_l(r)=D_1\exp(i\gamma r)+D_2\exp(-i\gamma r)$ and similarly for $S_l(r)$, we obtain the eigenvalues of the above equations $-\gamma^2=\kappa^2-g^2-\delta^2+2i\kappa g\cos(\theta_1-\theta_2)$. To ensure the same dispersion relation as that in a PT-symmetric planar Bragg grating, we should set $\theta_1=\theta_2\pm\pi/2$. Next, we focus our analysis on the 8th-order mode similar to that in Ref. [8].

Let us suppose the refractive index is n_{av} in the unperturbed region ($r<r_0$) and is expressed as follows in the perturbed region ($r_0<r<r_w$):

$$\begin{aligned}n=n_{\mathrm{av}}&+\Delta n_r\,\mathrm{sign}\{\cos[2\,\mathrm{phase}(H_8^{(1)}(k_{\mathrm{de}}r))+\theta_1]\}\\&+i\Delta n_i\,\mathrm{sign}\{\cos[2\,\mathrm{phase}(H_8^{(1)}(k_{\mathrm{de}}r))+\theta_2]\},\end{aligned} \tag{6}$$

where $\mathrm{sign}(x)$ is 1 for positive x and -1 for negative x, and r_w is the outer radius of the circular grating region. We also use N (the number of layers) to help describe the structure. Considering that $\Delta n(r)=\Delta n_r(r)+i\Delta n_i(r)$ and the perturbation is weak ($\Delta n_r,\ \Delta n_i\ll n_{\mathrm{av}}$), we can approximate $\Delta\varepsilon(r)$ as $2n_{\mathrm{av}}[\Delta n_r(r)+i\Delta n_i(r)]$ so that the Fourier

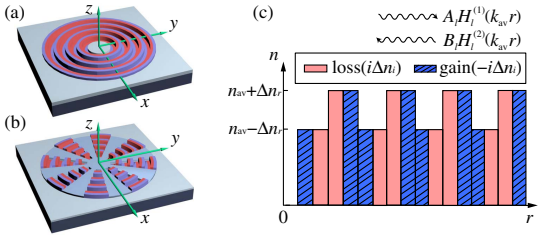

Fig. 1. (a) Schematic of the PT-symmetric circular Bragg laser. (b) Schematic of the azimuthally modulated circular Bragg laser with radial PT symmetry. (c) Radial profile of the refractive index of the two types of lasers, showing the real (Δn_r) and imaginary (Δn_i) refractive index modulations that satisfy the PT symmetry requirement.

expansion coefficients of $\Delta\varepsilon(r)$ respond linearly to $\Delta n(r)$. The index profile in Eq. (6) results in the Fourier expansion $\Delta\varepsilon(r) = \sum_{m=-\infty}^{\infty} a_m \exp[2mi\,\mathrm{phase}(H_8^{(1)}(k_{de}r))]$, where $a_0 = 0$, $a_1 = 4n_{av}[\exp(i\theta_1)\Delta n_r + i\exp(i\theta_2)\Delta n_i]/\pi$, $a_{-1} = 4n_{av}[\exp(-i\theta_1)\Delta n_r + i\exp(-i\theta_2)\Delta n_i]/\pi$. In this case, $\kappa = 2k_0\Delta n_r/\pi$ and $g = 2k_0\Delta n_i/\pi$. We obtain the solutions for the 8th-order mode

$$\begin{bmatrix} A_8(r_w) \\ B_8(r_w) \end{bmatrix} = \begin{bmatrix} M_{11}e^{-i\delta(r_w-r_0)} & M_{12}e^{-i\delta(r_w+r_0)} \\ M_{21}e^{i\delta(r_w+r_0)} & M_{22}e^{i\delta(r_w-r_0)} \end{bmatrix} \begin{bmatrix} A_8(r_0) \\ B_8(r_0) \end{bmatrix} \tag{7}$$

with

$$\begin{cases} M_{11} = \cosh(i\gamma L) + \delta\sinh(i\gamma L)/\gamma \\ M_{12} = (ie^{i\theta_1}\kappa - e^{i\theta_2}g)\sinh(i\gamma L)/i\gamma \\ M_{21} = (-ie^{-i\theta_1}\kappa + e^{-i\theta_2}g)\sinh(i\gamma L)/i\gamma \\ M_{22} = \cosh(i\gamma L) - \delta\sinh(i\gamma L)/\gamma \end{cases}. \tag{8}$$

Equation (8) reveals that, at the exceptional point ($\Delta n_r = \Delta n_i$), if $\theta_1 = \theta_2 - \pi/2$, then $M_{12} = 0$ and M_{11} is simplified as $\exp(i\delta L)$, yielding constant amplitude of the outward wave in the grating region. If $\theta_1 = \theta_2 + \pi/2$, then $M_{21} = 0$ and M_{22} is simplified as $\exp(-i\delta L)$, yielding constant amplitude of the inward wave. In what follows, we focus on the case of $\theta = \theta_1 = \theta_2 - \pi/2$.

Next, by applying the boundary conditions that the E field and its derivative must be continuous, and no inward wave should exist at $r = r_w$, we obtain the reflection coefficient of the circular Bragg grating at $r = r_0$, which is expressed as $\rho_r\exp(2i\delta r_0)$ with $\rho_r = -M_{21}/M_{22}$. We can further obtain the oscillation condition of circular Bragg lasers: $\rho_r\rho_0\exp(2i\delta r_0 + 2\alpha r_0) = 1$. ρ_0 denotes the reflection coefficient at $r = 0$, which must be equal to 1, and α is the gain coefficient in the central region. In circular Bragg lasers, the central region ($r < r_0$) provides the lasing modes with gain or loss to achieve the oscillation condition. Therefore, it is important to obtain the normalized threshold gain $\alpha r_0 = -\ln(|\rho_r\rho_0|)/2$, where the resonant wavelength should satisfy that $\mathrm{phase}(\rho_r) + 2\delta r_0$ be a multiple integer of 2π. For $\delta = 0$ and $\Delta n_r = \Delta n_i$, the reflection coefficient at $r = r_0$ can be simplified as $i(\kappa + g)L\exp(-i\theta)$, which scales linearly with the length of the grating region. Additionally, the laser can lase at the desired frequency when θ is equal to $\pi/2$. It should be noted that the PT symmetry can be realized only for the specific order of Fourier expansion of the refractive index, while the refractive index does not have to follow Eq. (6).

Now that we have designed radially chirped PT-symmetric circular Bragg lasers, we are ready to analyze the properties of their azimuthal modes. Due to different phase shifts in the approximation of even- and odd-order Hankel functions, the odd azimuthal modes are unlikely to be excited in lasers designed for even azimuthal modes [2]. By using the transfer-matrix method, which was verified by numerical solutions of the coupled equations, we calculated the normalized threshold gain (αr_0) for even azimuthal modes for two types of circular Bragg lasers, namely, conventional radially chirped and PT-symmetric radially chirped, with the results plotted in Fig. 2(a). Here "conventional" refers to a structure with $\Delta n_i = 0$ and $\Delta n_r = 0.08$, and "PT-symmetric" refers to a structure with $\Delta n_i = \Delta n_r = 0.025$, where a different Δn_r was chosen to ensure a similar threshold gain for the targeted mode operating at the wavelength of 1.55 μm for both types of lasers. Other structural parameters include $N = 120$, $n_{av} = 3.4$, and $r_0 = 1.164$ μm.

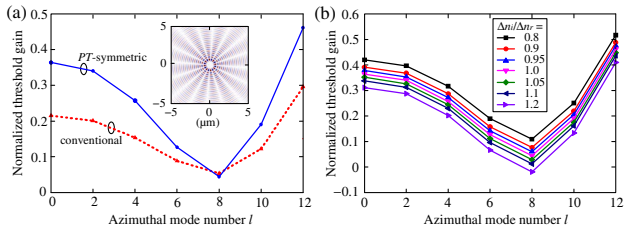

Fig. 2. (a) Normalized threshold gain (αr_0) for even-order azimuthal modes of PT-symmetric and conventional radially chirped circular Bragg lasers. Inset shows the E field profile of the targeted 8th-order azimuthal mode. (b) Effect of a small deviation away from the exceptional point on the normalized threshold gain values for the PT-symmetric radially chirped circular Bragg lasers.

As shown in Fig. 2(a), in both types of lasers, the intended 8th-order azimuthal mode indeed possesses the lowest threshold gain and thus will be the lasing mode. However, the PT-symmetric laser structure achieves larger modal discrimination (i.e., the difference of threshold gain between the lasing mode and the other modes) than the conventional counterpart. The bottom line is that the PT-symmetric circular Bragg lasers can be designed to optimize the performance of a mode of any azimuthal order, with significantly enhanced modal discrimination compared with the conventional circular Bragg lasers.

With the superior properties, the PT-symmetric circular Bragg lasers can be fabricated on a III–V wafer. Selective etching and metal deposition can modulate, respectively, the real (Δn_r) and the imaginary (Δn_i) part of the refractive index. This method was employed to fabricate the PT-symmetric microring laser, without the problem of carrier diffusion to destroy the PT symmetry [15,24]. The effect of a small deviation away from the exceptional point was also studied, where the imaginary part (Δn_i) and the real part (Δn_r) of the refractive index modulation are not equal. As shown in Fig. 2(b), increasing (decreasing) the imaginary modulation leads to an overall reduction (enhancement) of threshold gain for all modes, so the modal discrimination remains essentially unchanged.

3. CIRCULAR BRAGG LASERS WITH RADIAL PT SYMMETRY AND AZIMUTHAL MODULATION

In the previous section, a coupled-mode approach has been employed to analyze and design laser structures with modulation only in the radial direction. Because azimuthal modulation is usually employed to control azimuthal modes, in this section we propose to impose additional modulation in the azimuthal direction, as illustrated in Fig. 1(b). We will use the coupled-mode equations to analyze the modes and show the additional azimuthal modulation can also enhance the modal discrimination. To that end, we suggest the following refractive index profile:

$$n = n_{\mathrm{av}} - \Delta n_r \,\mathrm{sign}\{\sin[2\,\mathrm{phase}(H_8^{(1)}(k_{\mathrm{de}}r))]\}\Theta(\varphi) - i\Delta n_i \,\mathrm{sign}\{\cos[2\,\mathrm{phase}(H_8^{(1)}(k_{\mathrm{de}}r))]\}\Theta(\varphi) \quad (9)$$

with

$$\Theta(\varphi) = \begin{cases} 1, & \cos(q\varphi) > 0 \\ 0, & \cos(q\varphi) < 0 \end{cases},$$

where q denotes the number of periods in the azimuthal direction. The radial modulation in Eq. (9) is the same as that in Eq. (6). By following the approach in Ref. [8], under the weak perturbation condition, the responsible terms in the Fourier expansion of $\Delta\varepsilon(r,\varphi)$ are those of the 0th and 1st orders in the azimuthal direction and the 1st order in the radial direction. The azimuthal modulation defined by $\Theta(\varphi)$ actually introduces coupling between the lth- and $(l \pm q)$th-order azimuthal modes. From the previous work by Erdogan and Hall [2], we can analyze the structure with coupled-mode theory. For the PT-symmetric structure with refractive index defined in Eq. (9), the Fourier expansion of $\Delta\varepsilon(r)$ yields $\Delta\varepsilon(r,\varphi) = \sum_{h=-\infty}^{\infty}\sum_{f=-\infty}^{\infty} s_{f,h} e^{2hiq\varphi}\exp[2fi\,\mathrm{phase}(H_8^{(1)}(k_{\mathrm{de}}r))]$ with $s_{-1,0} = 2n_{\mathrm{av}}(\Delta n_r + \Delta n_i)/\pi$, $s_{-1,1} = s_{-1,-1} = 4n_{\mathrm{av}}(\Delta n_r + \Delta n_i)/\pi^2$, $s_{1,0} = 2n_{\mathrm{av}}(\Delta n_r - \Delta n_i)/\pi$, $s_{1,1} = s_{1,-1} = 4n_{\mathrm{av}}(\Delta n_r - \Delta n_i)/\pi^2$, and $f(h)$ being the order of Fourier expansion in the radial (azimuthal) direction. These parameters determine the coupling coefficients between the different modes. It should be noted that the coupling strength relies not only on the coefficient but also on an overlap integral involving the modal profiles in the radial direction. Without loss of generality, we choose $q = 16$, which leads to strong coupling between the 8th-order mode and the −8th-order mode, which have the same profile in the radial direction.

We compared the reflectivity of the same azimuthal mode for two laser structures (without and with azimuthal modulation) by solving the coupled-mode equations numerically. The two structures share the same r_0 (1.03 μm) and N (120). The modulation depth ($\Delta n_r = \Delta n_i$) is set to be 0.025 and 0.03 to ensure the same reflectivity of the 8th-order mode for the laser with and without the azimuthal modulation, respectively. Assuming that the amplitudes of the outward wave of different modes are the same, we can obtain the two highest-reflectivity modes of the PT-symmetric laser without azimuthal modulation: 0.804 for the 1st-order mode and 0.904 for the 8th-order mode. The reflectivity of the 8th-order mode of the structure with azimuthal modulation remains 0.904, but that of the 1st-order mode reduces to 0.366. This suppression is attributed mainly to the mismatch of the modal profiles between the 1st-order mode and the −15th-order mode in the radial direction. As previously mentioned, such analysis is based on a 2D model. Some other effects of azimuthal modulation are not considered here. For example, the diffracted waves can be coupled with radiation modes, which results in reduced modal discrimination [27].

We also simulated the two laser structures in Lumerical by an FDTD method [28]. Figure 3 plots the simulated laser output spectra with the modal field distribution for the resonant modes. As predicted by the coupled-mode theory, the 8th-order mode plays a major role, while the additional azimuthal modulation introduces significant mode suppression to the 1st-order mode. It is clear that the azimuthal modulation structures proposed in this section not only enjoy the benefit from the PT-symmetric radial gratings but also get further suppression to the unwanted modes from the deliberately designed azimuthal modulation.

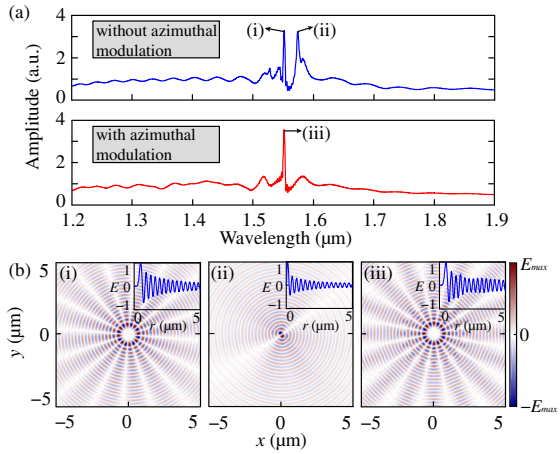

Fig. 3. (a) Output spectra for two circular Bragg laser structures with radial PT symmetry. The upper corresponds to the one without azimuthal modulation, while the lower corresponds to the one with azimuthal modulation. (b) E field profiles of the modes at the three peaks in the laser output spectra. Modes (i) and (ii) from the upper spectrum are of the 8th and 1st azimuthal order, respectively. Mode (iii) from the lower spectrum is of the 8th azimuthal order.

4. CONCLUSION

We have adopted a coupled-mode approach to design and analyze circular Bragg lasers with radial PT symmetry. We analyzed and compared the threshold gain for different azimuthal modes of circular Bragg lasers with radially chirped gratings for both conventional and PT-symmetric structures. We have shown that the PT-symmetric radially chirped circular Bragg lasers have higher modal discrimination. Further suppression to unwanted modes is obtained by introducing an additional azimuthal modulation to the circular Bragg lasers with radial PT symmetry. With an intrinsic broadside circular aperture, such lasers will lend themselves to a variety of applications in integrated photonic and optoelectronic circuitry as well as fiber-optic communication.

Funding. Hong Kong Research Grants Council Early Career Scheme (24208915); National Natural Science Foundation of China (NSFC) and Research Grants Council of Hong Kong Joint Research Scheme (N_CUHK415/15).

REFERENCES

1. K. J. Vahala, "Optical microcavities," Nature **424**, 839–846 (2003).
2. T. Erdogan and D. G. Hall, "Circularly symmetric distributed feedback semiconductor laser: an analysis," J. Appl. Phys. **68**, 1435–1444 (1990).
3. T. Erdogan and D. G. Hall, "Circularly symmetric distributed feedback laser: coupled mode treatment of TE vector fields," IEEE J. Quantum Electron. **28**, 612–623 (1992).

4. C. Wu, T. Makino, S. I. Najafi, R. Maciejko, M. Svilans, J. Glinski, and M. Fallahi, "Threshold gain and threshold current analysis of circular grating DFB and DBR lasers," IEEE J. Quantum Electron. **29**, 2596–2606 (1993).
5. X. M. Gong, A. K. Chan, and H. F. Taylor, "Lateral mode discrimination in surface emitting DBR lasers with cylindrical symmetry," IEEE J. Quantum Electron. **30**, 1212–1218 (1994).
6. A. Shaw, B. Roycroft, J. Hegarty, D. Labilloy, H. Benisty, C. Weisbuch, T. F. Krauss, C. J. M. Smith, R. Stanley, R. Houdré, and U. Oesterle, "Lasing properties of disk microcavity based on a circular Bragg reflector," Appl. Phys. Lett. **75**, 3051–3053 (1999).
7. J. Scheuer, "Radial Bragg lasers: optimal design for minimal threshold levels and enhanced mode discrimination," J. Opt. Soc. Am. B **24**, 2178–2184 (2007).
8. J. Scheuer and A. Yariv, "Coupled-waves approach to the design and analysis of Bragg and photonic crystal annular resonators," IEEE J. Quantum Electron. **39**, 1555–1562 (2003).
9. X. K. Sun and A. Yariv, "Modal properties and modal control in vertically emitting annular Bragg lasers," Opt. Express **15**, 17323–17333 (2007).
10. X. K. Sun and A. Yariv, "Surface-emitting circular DFB, disk-, and ring-Bragg resonator lasers with chirped gratings. II: nonuniform pumping and far-field patterns," Opt. Express **17**, 1–6 (2009).
11. C. M. Bender and S. Boettcher, "Real spectra in non-Hermitian Hamiltonians having PT symmetry," Phys. Rev. Lett. **80**, 5243–5246 (1998).
12. A. Guo, G. J. Salamo, D. Duchesne, R. Morandotti, M. Volatier-Ravat, V. Aimez, G. A. Siviloglou, and D. N. Christodoulides, "Observation of PT-symmetry breaking in complex optical potentials," Phys. Rev. Lett. **103**, 093902 (2009).
13. K. G. Makris, R. El-Ganainy, D. N. Christodoulides, and Z. H. Musslimani, "Beam dynamics in PT symmetric optical lattices," Phys. Rev. Lett. **100**, 103904 (2008).
14. C. E. Ruter, K. G. Makris, R. El-Ganainy, D. N. Christodoulides, M. Segev, and D. Kip, "Observation of parity-time symmetry in optics," Nat. Phys. **6**, 192–195 (2010).
15. L. Feng, Z. J. Wong, R.-M. Ma, Y. Wang, and X. Zhang, "Single-mode laser by parity-time symmetry breaking," Science **346**, 972–975 (2014).
16. J. H. Gu, X. Xi, J. W. Ma, Z. J. Yu, and X. K. Sun, "Parity-time-symmetric circular Bragg lasers: a proposal and analysis," Sci. Rep. **6**, 37688 (2016).
17. Y. Zhu, Y. Zhao, J. Fan, and L. Zhu, "Modal gain analysis of parity-time-symmetric distributed feedback lasers," IEEE J. Sel. Top. Quantum Electron. **22**, 5–11 (2016).
18. H. Hodaei, M.-A. Miri, M. Heinrich, D. N. Christodoulides, and M. Khajavikhan, "Parity-time-symmetric microring lasers," Science **346**, 975–978 (2014).
19. M. Kulishov, B. Kress, and R. Slavík, "Resonant cavities based on Parity-Time-symmetric diffractive gratings," Opt. Express **21**, 9473–9483 (2013).
20. H. Hodaei, A. U. Hassan, W. E. Hayenga, M. A. Miri, D. N. Christodoulides, and M. Khajavikhan, "Dark-state lasers: mode management using exceptional points," Opt. Lett. **41**, 3049–3052 (2016).
21. K.-H. Kim, M.-S. Hwang, H.-R. Kim, J.-H. Choi, Y.-S. No, and H.-G. Park, "Direct observation of exceptional points in coupled photonic-crystal lasers with asymmetric optical gains," Nat. Commun. **7**, 13893 (2016).
22. M. Brandstetter, M. Liertzer, C. Deutsch, P. Klang, J. Schöberl, H. E. Türeci, G. Strasser, K. Unterrainer, and S. Rotter, "Reversing the pump dependence of a laser at an exceptional point," Nat. Commun. **5**, 4034 (2014).
23. M. Liertzer, L. Ge, A. Cerjan, A. D. Stone, H. E. Türeci, and S. Rotter, "Pump-induced exceptional points in lasers," Phys. Rev. Lett. **108**, 173901 (2012).
24. P. Miao, Z. Zhang, J. Sun, W. Walasik, S. Longhi, N. M. Litchinitser, and L. Feng, "Orbital angular momentum microlaser," Science **353**, 464–467 (2016).
25. M. Kulishov, J. M. Laniel, N. Bélanger, J. Azaña, and D. V. Plant, "Nonreciprocal waveguide Bragg gratings," Opt. Express **13**, 3068–3078 (2005).
26. Z. Lin, H. Ramezani, T. Eichelkraut, T. Kottos, H. Cao, and D. N. Christodoulides, "Unidirectional invisibility induced by PT-symmetric periodic structures," Phys. Rev. Lett. **106**, 213901 (2011).
27. M. Fujita and T. Baba, "Proposal and finite-difference time-domain simulation of whispering gallery mode microgear cavity," IEEE J. Quantum Electron. **37**, 1253–1258 (2001).
28. www.lumerical.com/tcad-products/fdtd/.